

PROCEEDINGS OF SPIE

[SPIDigitalLibrary.org/conference-proceedings-of-spie](https://spiedigitallibrary.org/conference-proceedings-of-spie)

3-D Reconstruction Of Vessels With Stenoses And Aneurysms From Dual Bi-Plane Angiograms

Jeffrey A. Fessler, Albert Macovski

Jeffrey A. Fessler, Albert Macovski, "3-D Reconstruction Of Vessels With Stenoses And Aneurysms From Dual Bi-Plane Angiograms," Proc. SPIE 1092, Medical Imaging III: Image Processing, (25 May 1989); doi: 10.1117/12.953241

SPIE.

Event: Medical Imaging III, 1989, Newport Beach, CA, United States

3-D Reconstruction of Vessels with Stenoses and Aneurysms from Dual Bi-Plane Angiograms

Jeffrey A. Fessler and Albert Macovski*
Information Systems Laboratory
Department of Electrical Engineering
Stanford University · Stanford, CA 94305

Abstract

Parametric model-based approaches to 3-D reconstruction of vessels overcome the inherent problem of underdeterminacy in reconstruction from limited views by incorporating *a priori* knowledge about the structure of vessels and about the measurement statistics. In this paper, we describe two extensions to the parametric approach. First, we consider the problem of reconstruction from a pair of bi-plane angiograms that are acquired at different projection angles. Since bi-plane angiography systems are widely available, this is a practical measurement geometry. The patient may move between acquisitions, so we have extended our model to allow for object translation between the first and second pair of projections. Second, we describe how to accurately estimate the dimensions of an aneurysm from the dual-biplane angiogram.

We applied the new algorithm to four synthetic angiograms (projection angles 0° , 20° , 90° , and 110°) of a vessel with a small aneurysm and an eccentric stenosis. The angiograms were corrupted by additive noise and background structure. Except near the top and bottom of the aneurysm, the estimated cross sections of the aneurysm and stenosis agree very well with the true cross sections.

1. INTRODUCTION

3-D reconstruction of arterial trees from a few projections is important for quantitative diagnosis and for surgical planning. Reconstruction from limited projections is severely underdetermined in general, which leads to unacceptable artifacts in images reconstructed by conventional approaches. When the projected objects are blood vessels, one can overcome this problem by incorporating *a priori* knowledge about their structure. Non-parametric reconstruction approaches incorporate constraints such as positivity, connectedness, boundedness, and sparseness. These methods are better than conventional methods, but they still require many views. In applications where only a few views are available, parametric model-based reconstruction approaches [1, 2, 3, 4, 5] seem the most promising.

Parametric approaches are based on 3-D modeling of objects (vessel trees). By combining an object model with a statistical model for projection imaging, one can formulate the reconstruction problem as a Maximum Likelihood (ML) estimation problem. This estimation problem can be efficiently solved with a hierarchical algorithm for multiple object reconstruction [6, 7]. Parametric approaches have the advantage that important diagnostic factors such as percent stenosis can be directly computed from the reconstruction.

We use an elliptical model for vessel cross sections. Bresler [8] has shown that reconstruction of an arbitrary ellipse distribution requires at least three views, but his analysis was for ideal projections. Our experience has been that at least four views are needed, since real images are corrupted by noise, blurring, and background structures. Note that in some applications, only the transverse areas and skeletons of the vessel tree may be needed. These quantities can be computed from only two views [5].

In this paper we describe an algorithm for vessel reconstruction from a particular arrangement of four views that we call "dual bi-plane angiograms," two bi-plane angiogram pairs acquired at different projection angles. Bi-plane angiography systems are widely available; they consist of two X-ray source-detector pairs that are (almost)

*This work was supported in part by the National Institute of Health under contract NO1-HV-38045 and grant R01-HL-38045, National Science Foundation contract ECS-8213959, and General Electric contract 22-84.

simultaneously activated to acquire two orthogonal views. We assume that two views are acquired at angles 0° and 90° , the X-ray gantry is rotated by θ_r , and two more views are acquired at angles θ_r and $90^\circ + \theta_r$. For the example presented in Section 5, we used $\theta_r = 20^\circ$. More experimentation is needed to determine the minimum rotation angle.

Ideally, the patient would be motionless between the two acquisitions. Since this is not realistic, we have extended our model to allow for lateral translation of the vessels between the acquisitions. In this paper, we demonstrate that the parametric reconstruction paradigm easily accommodates the two additional degrees of freedom due to the translation. For the best results, one should still minimize vessel motion by gating the acquisitions to the heart, and by performing the acquisitions within a breath holding interval.

If the X-ray gantry rotates too slowly, two contrast agent injections may be required. The imaged vessels could then have different contrast densities in the two acquisitions. This additional degree of freedom could also be incorporated into the model, though we do not do so here.

In this paper we also present an algorithm for reconstruction of vessels with aneurysms. An aneurysm is a sac formed by local enlargement of the weakened wall of an artery. Interventional procedures, such as detachable embolization, where small balloons are left inflated within an aneurysm, would benefit from a quantitative description of the aneurysm geometry. Although aneurysms can be quite irregularly shaped, the elliptical model is sufficient for determining balloon size and placement.

To simplify notation, we describe the algorithm for reconstruction of a single vessel with a single aneurysm. The full hierarchical approach [7] to multiple object estimation can be applied when it is not possible to isolate a single vessel.

In Sections 2 and 3, we describe the object model and the measurement model. In Section 4 we outline the algorithm for reconstructing a vessel with an aneurysm. In Section 5 we discuss the results of a phantom study.

2. OBJECT MODEL

Vessels are well modeled as generalized cylinders [9], a collection of stacked primitives. A primitive is a “pill box” with an elliptical cross section and with a height that depends on the imaging resolution (usually 1 pixel). The elliptical cross section model is a reasonable tradeoff between simplicity and versatility. Pappas [4] has demonstrated the accuracy of the elliptical model by comparing the cross sections of excised stenotic vessels with their best fit ellipses. Though the accuracy of the elliptical model will decrease if the vessels are tilted severely away from vertical, proper positioning of the patient can minimize this problem.

An elliptical primitive has three shape parameters: radius, eccentricity, and orientation, denoted r, λ , and ϕ respectively. Let $\psi = [r \ \lambda \ \phi]$. To allow for changing bolus concentration, each primitive has its own linear attenuation coefficient, denoted α . The vertical position of a primitive is denoted by the index z , where $z = 1$ is the top scan line of the projections, and $z = N$ is the bottom scan line. Let (C_x, C_y) denote the coordinates of the center of the primitive during first bi-plane acquisition, and let $(C_x + \Delta_x, C_y + \Delta_y)$ denote the coordinates for the second bi-plane acquisition, where (Δ_x, Δ_y) is the unknown lateral translation. We use $\mathbf{P}(z)$ to denote the eight parameters of the elliptical cross section of the vessel at slice z , i.e., $\mathbf{P}(z) = [C_x(z) \ \Delta_x(z) \ C_y(z) \ \Delta_y(z) \ \psi(z) \ \alpha(z)] \triangleq [p_1(z) \ \dots \ p_8(z)]$.

An object is defined by a set of primitives with an index set that indicates the extent of the object. Let $S_v = \{\mathbf{P}_v(z) : z \in Z_v\}$, where $Z_v = \{1, \dots, N\}$. S_v is the set of (unknown) primitive parameters for the vessel. (For simplicity, we assume the vessel transverses the entire image.) We consider the aneurysm to be a separate object, and denote its set of primitive parameters by $S_a = \{\mathbf{P}_a(z) : z \in Z_a\}$, where $Z_a = \{z_1, \dots, z_2\}$. z_1 and z_2 are the top and bottom indices of the aneurysm. In the current implementation, these indices must be identified by the user, which is easily done with a mouse and cross-hairs on a video display.

Blood vessels are smoothly shaped objects, which means that the primitive parameters $\mathbf{P}(z)$ are smooth functions of z . An effective reconstruction method must incorporate this *a priori* knowledge into its object model. Our approach [10] is to use an object prior that is based on the non-parametric “roughness penalty” formulation of cubic-spline smoothing [11], and on the regularization ideas of machine vision [12]. If an object is composed of a set S of primitives with index set Z , $S = \{\mathbf{P}(z) : z \in Z\}$, then the object likelihood is

$$L_O(S) = - \sum_{i=1}^8 w_i \int_{\min(Z)}^{\max(Z)} \ddot{p}_i^2(z) dz. \quad (1)$$

This prior assigns the highest likelihood to the smoothest objects, since the second derivative is related to curvature. This is not to say that wiggly objects will be excluded; in fact, the weights w_i will be determined from the data itself (Appendix B). Thus the algorithm will adapt to vessel abnormalities such as stenoses.

3. MEASUREMENT MODEL

In this section, we present a statistical model for the projection measurements. We assume that the measurements are line-integral projections from a point source. We account for the lateral magnification due to the point source, but neglect the vertical magnification, requiring that the object be approximately centered vertically. The projections are assumed to be digitized images of dimension $N \times T$ pixels. We use $y_\theta(t; z)$ to denote the measured projection at angle θ , with the convention that the index t varies from $-T/2$ to $T/2$ across each row of the image. The measurement model is identical for each slice, so we drop the vertical index z in the description below.

Fig. 1 shows the ideal dual bi-plane projections of a primitive with parameters $\mathbf{P} = [C_x \ \Delta_x \ C_y \ \Delta_y \ r \ \lambda \ \phi \ \alpha]$. Each signal $s_{\theta_m}(t; \mathbf{P})$ is a semi-ellipse pulse that is offset from the center of the projection by τ_m , where

$$\tau_m \triangleq \tau(x_m, y_m, \theta_m), \quad (2)$$

$$\theta_1 \triangleq 0^\circ, \theta_2 \triangleq 90^\circ, \theta_3 \triangleq \theta_r, \theta_4 \triangleq 90^\circ + \theta_r,$$

$$x_1 = x_2 = C_x, \ x_3 = x_4 = C_x + \Delta_x, \ y_1 = y_2 = C_y, \ y_3 = y_4 = C_y + \Delta_y,$$

$$\tau(x, y, \theta) = M(x, y, \theta) \cdot (x \sin(\theta) - y \cos(\theta)),$$

and

$$M(x, y, \theta) = \frac{s_d}{s_o + (x \cos(\theta) + y \sin(\theta))}.$$

M is the position dependent magnification due to the point source model. s_d is the source-to-detector distance. s_o is the distance from the source to the rotational center of the gantry (coordinate (0,0) in Fig. 1). The mathematical form of the ideal projection at angle θ_m is

$$s_{\theta_m}(t; \mathbf{P}) = \alpha \cdot g_{\theta_m}(t - \tau_m; \mathbf{P}), \quad (3)$$

$$g_{\theta_m}(t; \mathbf{P}) = l_{\theta_m}(\psi) \sqrt{1 - \left(\frac{t}{M(x_m, y_m, \theta_m) a_{\theta_m}(\psi)} \right)^2} \Pi \left(\frac{t}{2M(x_m, y_m, \theta_m) a_{\theta_m}(\psi)} \right),$$

where $a_\theta(\psi) = r\sqrt{A_\theta(\psi)}$, $l_\theta(\psi) = 2r/\sqrt{A_\theta(\psi)}$, $A_\theta(\psi) = [(\lambda + 1/\lambda) - (\lambda - 1/\lambda) \cos(2(\phi - \theta))]/2$, and $\Pi(x) = 1_{\{|x| < 1/2\}}$.

The actual measured projections suffer from blurring, undesirable background structures, and measurement noise. These aberrations are captured by the following measurement model for the projection at angle θ :

$$y_\theta(t) = s_\theta(t; \mathbf{P}) * h(t) + b_\theta(t) + v_\theta(t), \quad (4)$$

where $h(t)$ is the imaging point spread function, $b_\theta(t)$ is an unknown smoothly varying background, and $v_\theta(t)$ is additive white Gaussian noise (AWGN) with (possibly unknown) variance σ^2 .

The choice of background model b_θ determines the applicability of the reconstruction algorithm described in the next section [10]. We assume that b_θ is varying smoothly, so that *locally* (i.e., near the projection g_θ), it can be well approximated by a line. If the pulse g_θ is centered about τ , then we assume

$$b_\theta(t) = \begin{cases} \beta_\theta, & |t - \tau| < W \\ \text{arbitrary,} & \text{otherwise} \end{cases}, \quad (5)$$

where W is a constant that is slightly larger than the radius of the largest possible vessel¹. Let $\beta = [\beta_{\theta_1} \ \dots \ \beta_{\theta_4}]$.

Because of the AWGN model (4), the likelihood of a particular primitive \mathbf{P} and set of background coefficients β , given the primitive's four projections, is the squared error between the measured projections and the projections

¹It may seem like a better background model would include an affine term as well as the DC term. In fact, the two models result in identical estimation algorithms. Since the semi-ellipse function is symmetric, it is orthogonal to affine functions [10].

computed from the parameters using (3), (4), and (5). The background coefficients are nuisance parameters, so we define the primitive likelihood to be

$$L_P(\mathbf{P}(z) | Y(z)) = -\min_{\beta} \sum_{m=1}^4 \int_{I_m} |y_{\theta_m}(t; z) - \alpha g'_{\theta_m}(t - \tau_m; \mathbf{P}(z)) - \beta_{\theta_m}|^2 dt, \quad (6)$$

where $I_m = [\tau_m - W, \tau_m + W]$, $Y(z) = \{y_{\theta_m}(t; z)\}_{m=1}^4$, and $g'_{\theta_m} = g_{\theta_m} * h$. This measure assigns the highest likelihood to the primitives whose projections best agree with the measurements.

Since we assume the measurement noise is independent from line to line, the measurement likelihood of a set of primitives S with index set Z is

$$L_M(S) = \sum_{z \in Z} L_P(\mathbf{P}(z) | Y(z)). \quad (7)$$

4. RECONSTRUCTION ALGORITHM

4.1. Single object reconstruction

Consider first the problem of reconstructing a single object, with primitive set S and index set Z , from its projections. Combining the object and measurement model described above, one can show the reconstruction problem is equivalent to the problem of finding the set of primitives that maximize the sum of the object likelihood (1) and the measurement likelihood (7):

$$\hat{S}_{ML} = \arg \max_S L_O(S) + L_M(S | \{Y(z) : z \in Z\}).$$

This solution is globally optimal [3], but it is impractical to compute since the parameter space is very large. Instead, we use a two step procedure, similar to the hierarchical algorithm of Bresler [7]:

$$\begin{aligned} \hat{S} &= \arg \max_S L_M(S), \\ \hat{S} &= \arg \max_S L_O(S) - \|\hat{S} - S\|, \end{aligned} \quad (8)$$

where $\|\hat{S} - S\| = \sum_{z \in Z} \sum_{p=1}^8 |\hat{x}_p - x_p|^2$. The first step is to maximize the measurement likelihood of the primitives. Since the measurements are independent (7), each primitive is estimated independently using the procedure given in Appendix A. Since the object smoothness prior has not been incorporated, these primitive estimates will be rough. The second step is then to smooth the initial set of primitives, using the spline smoothing algorithm described in Appendix B. We have shown empirically that this approach compares favorably with an optimal algorithm [6].

4.2. Reconstruction of a vessel with an aneurysm

The two step procedure (8) is easily adapted to the problem of reconstruction of a vessel with an aneurysm. The key is that spline smoothing can be applied even when the measurement samples are non-uniform or have gaps. This suggests the following algorithm for reconstruction with aneurysms:

- $\hat{S}_v = \arg \max_S L_M(S | \{Y(z) : z \in Z_v \ \& \ z \notin Z_a\})$. Apply the procedure in Appendix A to find the ML vessel primitive estimates on all slices except where the aneurysm is located.
- $\hat{S}_v = \arg \max_S L_O(S) - \|\hat{S}_v - S\|$. Smooth the vessel primitive parameter estimates using the spline smoothing algorithm of Appendix B.
- $Y'(z) = Y(z) - \text{Projection}(\hat{\mathbf{P}}_v(z))$, $z \in Z_v$. Subtract the computed projections of the estimated vessel from the angiograms.
- $\hat{S}_a = \arg \max_S L_M(S | \{Y'(z) : z \in Z_a\})$. Estimate the aneurysm primitives from the modified angiograms.
- $\hat{S}_a = \arg \max_S L_O(S) - \|\hat{S}_a - S\|$. Smooth the aneurysm estimates.

The vessel and aneurysm estimates, \hat{S}_v and \hat{S}_a , are the final parametric reconstruction. The estimated objects can be reprojected in any direction, displayed in a 3-D format, displayed in cross section, and used for quantitative diagnosis and surgical planning. Cross sections perpendicular to the vessel axis can also be computed from the estimates.

5. PHANTOM STUDY

We applied the above algorithm to synthetic angiograms of a vessel with an eccentric stenosis and a small aneurysm. The true primitive parameters were generated by hand, and the ideal projections were computed using (3). We added pseudo-random Gaussian noise with variance 4 to the projections. We also added a smoothly varying background (a 2-D Gaussian function) to simulate the intensity falloff that often occurs in real angiograms. Fig. 2 shows one of the two pairs of bi-plane angiograms. Each projection image is 128×128 pixels. For the other pair, at angles 20° and 110° the objects were shifted by $\Delta_x = 6$ and $\Delta_y = 8$ pixels. The signal to noise ratio of the data, defined by $l_{\psi}(\theta)/\sigma$, is about 5. At this signal to noise ratio, non-parametric approaches based on numerical derivatives would be biased [4]. The execution time for the algorithm was about five minutes on a Sun 3.

Figs. 2–6 illustrate the progress of the reconstruction algorithm. From a video display, it was clear that the aneurysm is limited to scan lines $z = 106, \dots, 113$. Fig. 3 shows the initial primitive estimates for the other scan lines. Projections of the smoothed vessel estimates are shown in Fig. 4. These projections were subtracted from the original angiograms, resulting in Fig. 5. The total disappearance of the vessel is evidence of the accuracy of the reconstruction. A 3-D display of the reconstruction is currently unavailable, but the outline of the reprojection of the reconstructed objects (in black) is superimposed on the projections of the true objects in Fig. 6. For diagnosis, the most useful displays are probably Fig. 7 and Fig. 8, which compare the true and estimated cross sections of the aneurysm and of the vessel stenosis. The average percentage error in the aneurysm area for the middle six slices was 6.0%, but the error was much higher for the outermost cross sections, where the ellipse is only 4 or 5 pixels across. For these cross sections, the SNR is only about 2.

Appendix A. SINGLE PRIMITIVE ESTIMATION

In this appendix we describe the procedure for estimating a primitive from its four projections. Since we are considering only a single slice, the index z is dropped. Given projections $Y = \{y_{\theta_m}\}_{m=1}^4$, the goal is to find the primitive parameters \mathbf{P} that maximize the primitive measurement likelihood (6). We will also have to estimate the nuisance parameters β .

There are eight primitive parameters and four background coefficients to estimate, so a global parameter search is impractical. Furthermore, since the support of the semi-ellipse functions is only a small fraction of each measured projection, the likelihood space has many flat regions that confound conventional hill climbing algorithms. Therefore, one must use a maximization procedure tailored to this problem.

Fortunately, the background coefficients and the attenuation α are all quadratic in (6), so we can solve for them analytically in terms of the other parameters and substitute the expressions back into (6). The result is that the ML estimates of \mathbf{P} maximize

$$\sum_{m=1}^4 (E_m(y_{\theta_m}) - A_m^2(y_{\theta_m})) - \frac{(\sum_{m=1}^4 \int_{I_m} y_{\theta_m}(t) g'_{\theta_m}(t - \tau_m; \mathbf{P}) dt - A_m(g'_{\theta_m}(t - \tau_m; \mathbf{P})) A_m(y_{\theta_m}))^2}{\sum_{m=1}^4 E(g'_{\theta_m}(t - \tau_m; \mathbf{P})) - A_m(g'_{\theta_m}(t - \tau_m; \mathbf{P}))^2}, \quad (9)$$

where

$$A_m(f) = \frac{1}{\sqrt{2W}} \int_{I_m} f(t) dt, \text{ and } E_m(f) = \frac{1}{2W} \int_{I_m} f^2(t) dt.$$

For efficiency, the terms involving only g_{θ_m} are precomputed using (3).

We have found empirically that the position estimates $(C_x, C_y, \Delta_x, \Delta_y)$ are insensitive to errors in the shape estimates (ψ) . Therefore (9) can be efficiently maximized by using the following procedure:

- Initialize the shape estimate ψ using the shape estimate from the previous slice.
- Maximize (9) over the position parameters: C_x, C_y, Δ_x , and Δ_y .
- Fine tune the shape estimate using the new position estimates.

The second step of this procedure has been studied by Rossi [2], in the case where $\Delta_x = \Delta_y = 0$ (no primitive movement allowed). In this case, the second step involves a form of (likelihood) convolution backprojection. Each projection is convolved with the semi-ellipse pulse g'_{θ_m} , and the result is backprojected. The position of peak of the backprojection is the ML estimate of (C_x, C_y) . In our case, there are four position parameters C_x, C_y, Δ_x and Δ_y , and four shift parameters τ_1, \dots, τ_4 , which have a one-to-one correspondence (2). Hence, finding the best position parameters for the second step of the procedure given above is equivalent to finding the best set of τ_m 's. The ML estimate of τ_m is the position of the peak of the convolution of g'_{θ_m} with y_{θ_m} , i.e., the classical matched filter. This operation is easier to compute than the convolution backprojection. Thus, although we have complicated the object model by allowing primitive translation, the resulting estimation algorithm is simplified. However, to achieve the same estimation accuracy, a higher signal-to-noise ratio is required in our case, since we are estimating more parameters.

Appendix B. SMOOTHING PRIMITIVE ESTIMATES

In this appendix, we show that the second step of procedure (8) is equivalent to spline smoothing of the parameter estimates. In general, given a set of data pairs (z, f_z) , an index set Z , and the model $f_z = g(z) + \eta_z$, where η_z is normally distributed measurement error, the smoothing-spline estimate [11] of g is

$$\hat{g} = \arg \min_g \sum_{z \in Z} |f_z - g(z)|^2 + w \int_{\min(Z)}^{\max(Z)} \ddot{g}^2(z) dz.$$

The minimizing function \hat{g} is a natural cubic spline, and can be easily computed [13]. The weight w is determined using cross validation or related methods [11, 14]. Since cubic splines are piecewise cubic polynomials, we can evaluate the estimate \hat{g} at all values of z , not just the values in Z .

By the definitions of L_O and $\|\hat{S} - S\|$,

$$\hat{S} = \arg \max_S L_O(S) - \|\hat{S} - S\|$$

is equivalent to

$$\hat{P} = \arg \min_P \sum_{i=1}^8 \sum_{z \in Z} |p_i(z) - \hat{p}_i(z)|^2 + \sum_{i=1}^8 w_i \int_{\min(Z)}^{\max(Z)} \ddot{p}_i^2(z) dz. \quad (10)$$

Since ML estimates $\hat{p}_i(z)$ are approximately normally distributed, (10) is equivalent to eight spline smoothing problems, one for each parameter. This is the approach used for the simulation. We are currently investigating a new approach that would simultaneously smooth all the parameters [15].

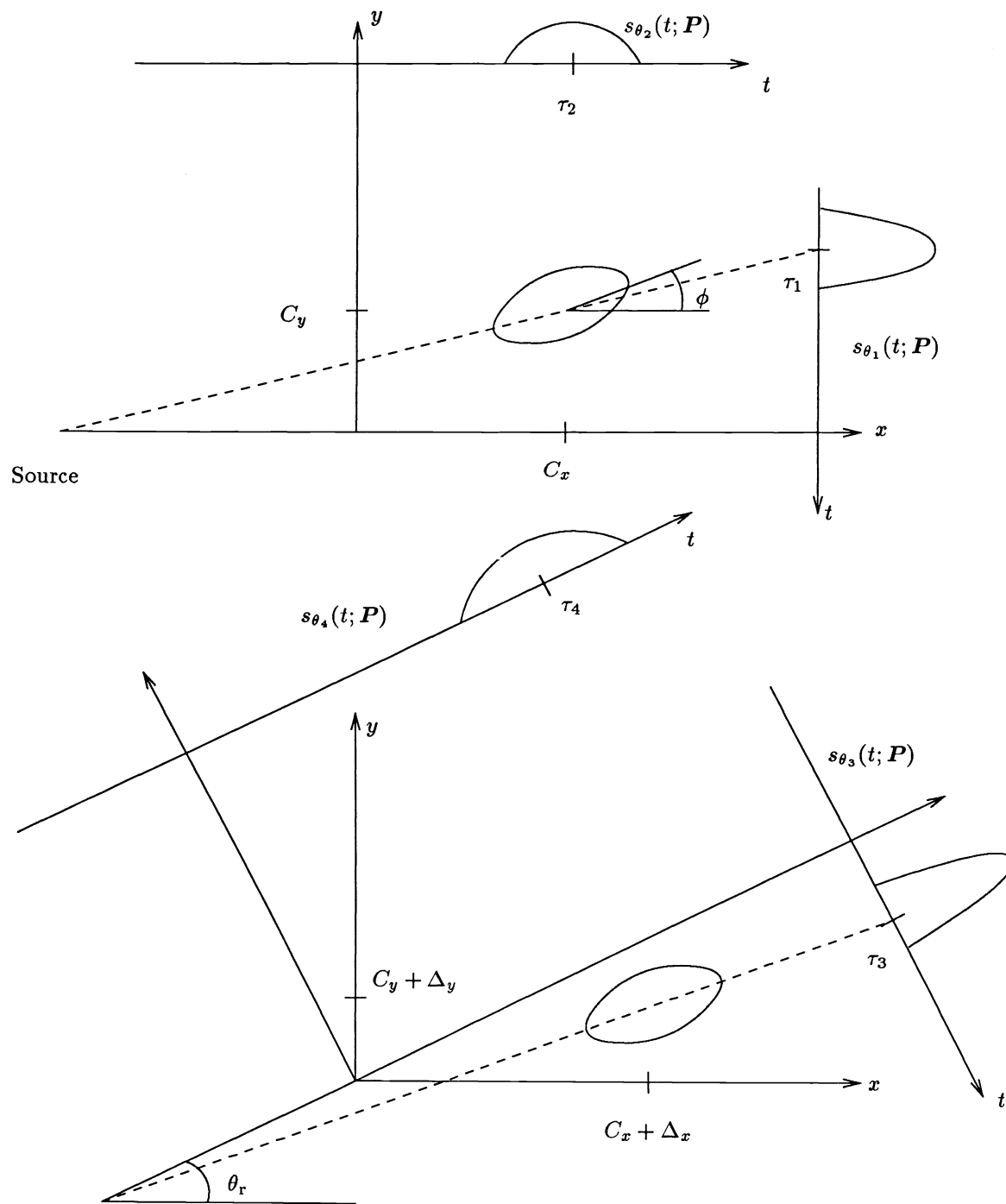


Figure 1: Dual bi-plane projections of an elliptical primitive.

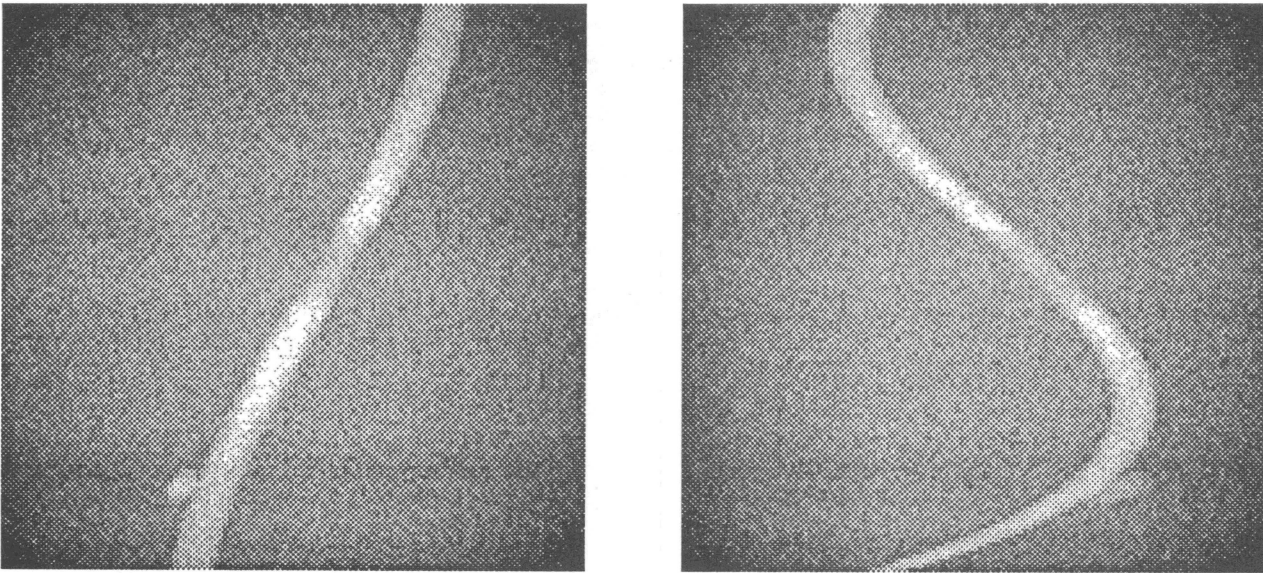


Figure 2: One of the two pairs of simulated bi-plane angiograms. Left: $\theta = 0^\circ$, right: $\theta = 90^\circ$.

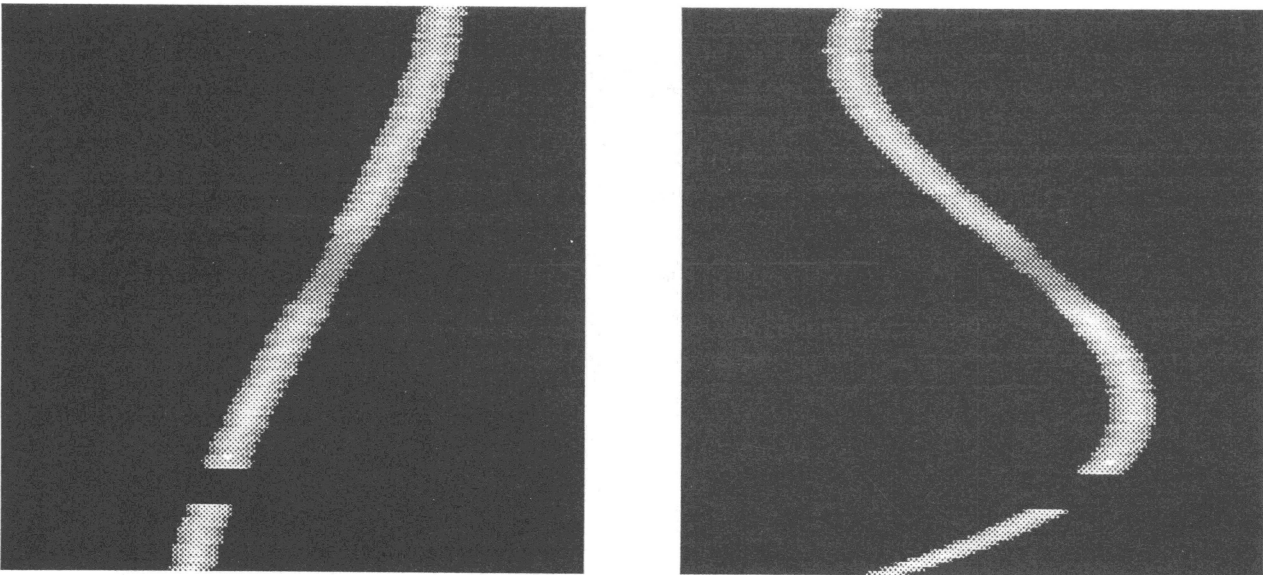


Figure 3: Projections of vessel primitive estimates \hat{S}_v before smoothing. Left: $\theta = 0^\circ$, right: $\theta = 90^\circ$.

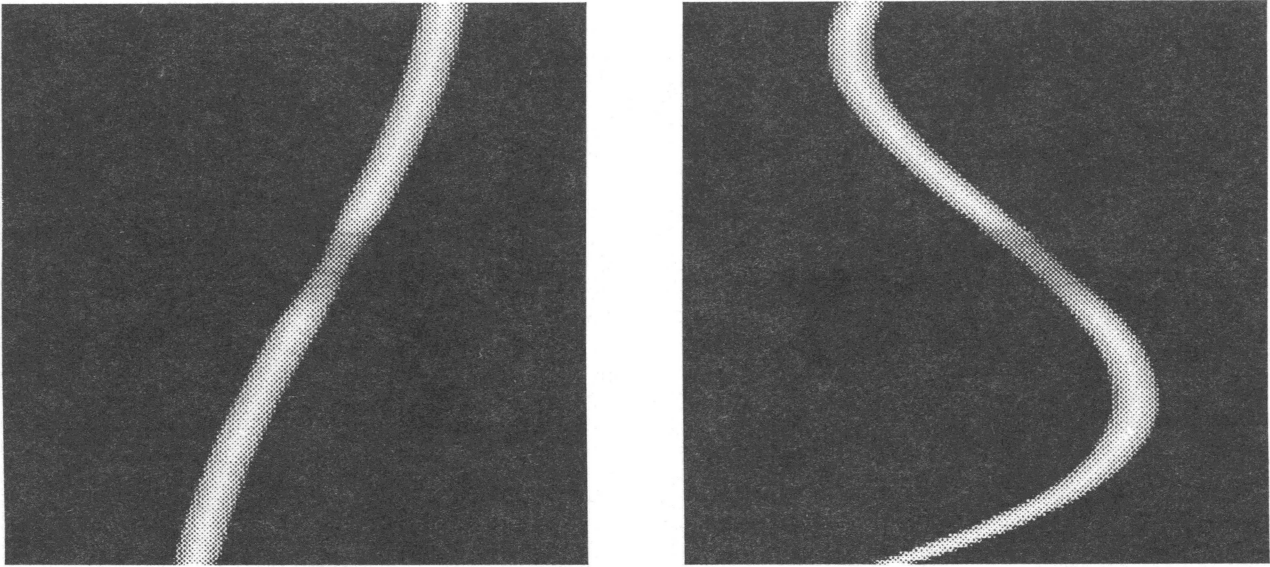


Figure 4: Projections of vessel primitive estimates \hat{S}_v after smoothing. Left: $\theta = 0^\circ$, right: $\theta = 90^\circ$.

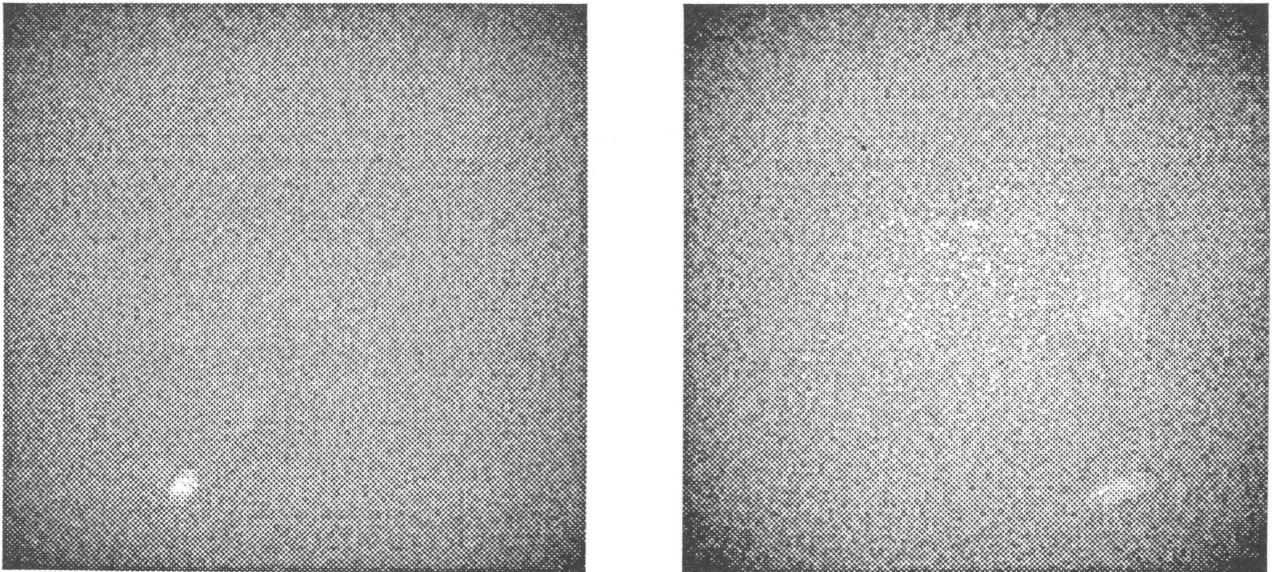


Figure 5: Difference between original angiograms and smoothed vessel estimates. Left: $\theta = 0^\circ$, right: $\theta = 90^\circ$.



Figure 6: Outline of reprojection of estimated vessel and aneurysm (black) superimposed on true objects (shaded). Left: $\theta = 0^\circ$, right: $\theta = 90^\circ$.

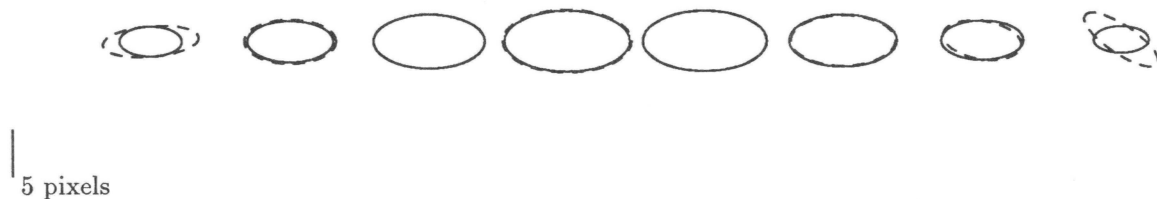


Figure 7: True (solid) vs. estimated (dashed) aneurysm cross sections, $z = 106, \dots, 103$.

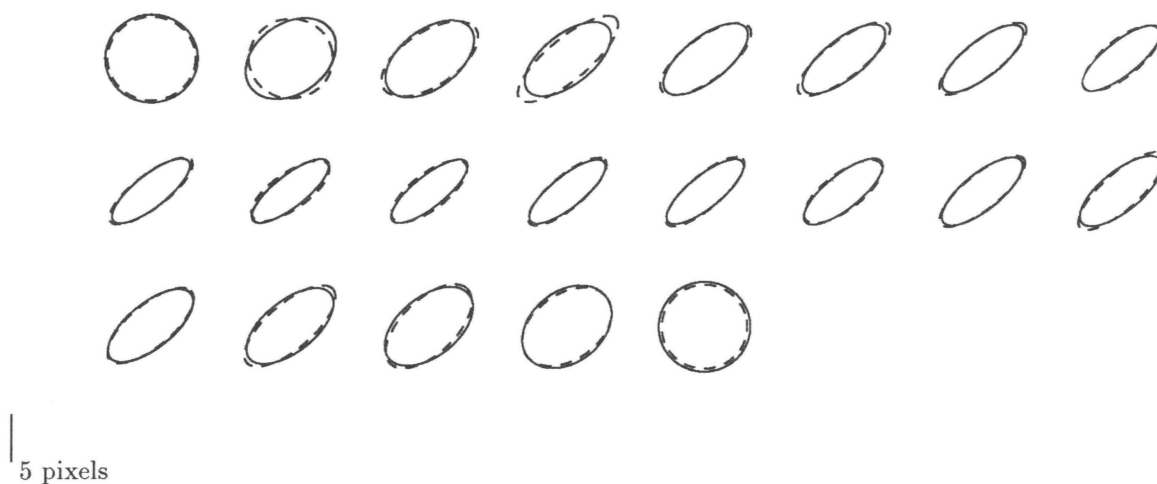


Figure 8: True (solid) vs. estimated (dashed) stenosis cross sections, $z = 50, \dots, 70$.

*References

- [1] K. Shmueli, W. Brody, and A. Macovski, "Estimation of blood vessel boundaries in X-ray images," *Optical Engineering*, vol. 22, pp. 110–116, Jan. 1983.
- [2] D. Rossi and A. Willski, "Reconstruction from projections based on detection and estimation of objects—parts I & II: performance analysis and robustness analysis," *IEEE Transactions on Acoustics Speech and Signal Processing*, vol. 32, pp. 886–906, Aug. 1984.
- [3] Y. Bresler and A. Macovski, "Three-dimensional reconstruction from projections with incomplete and noisy data by object estimation," *IEEE Transactions on Acoustics Speech and Signal Processing*, vol. 35, pp. 1139–1152, Aug. 1987.
- [4] T. Pappas and J. Lim, "A new method for estimation of coronary artery dimensions in angiograms," *IEEE Transactions on Acoustics Speech and Signal Processing*, vol. 36, pp. 1501–1513, Sep. 1988.
- [5] K. Kitamura, J. Tobis, and J. Sklansky, "Estimating the 3-D skeletons and transverse areas of coronary arteries from biplane angiograms," *IEEE Transactions on Medical Imaging*, vol. 7, pp. 173–187, Sep. 1988.
- [6] Y. Bresler, J. Fessler, and A. Macovski, "Model based estimation techniques for 3-D reconstruction from projections," *Machine Vision and Applications*, vol. 1, pp. 115–126, 1988.
- [7] Y. Bresler, J. Fessler, and A. Macovski, "A Bayesian approach to reconstruction from incomplete projections of a multiple object 3-D domain," *IEEE Transactions on Pattern Analysis and Machine Intelligence*, 1989. To appear.
- [8] Y. Bresler, *Model Based Estimation Techniques for 3-D Reconstruction from Projections*. PhD thesis, Stanford University, Stanford, CA., Dec. 1985.
- [9] G. Agin and T. Binford, "Computer description of curved objects," *IEEE Transactions on Computers*, vol. C-25, pp. 439–449, Apr. 1976.
- [10] J. Fessler and A. Macovski, "3-D reconstruction of vessel trees from a few projections - a phantom study," 1989. submitted to IEEE Conf. on Computer Vision and Pattern Recognition.
- [11] B. Silverman, "Some aspects of the spline smoothing approach to non-parametric regression curve fitting," *Journal of the Royal Statistical Society Series B*, vol. 47, pp. 1–52, 1985.
- [12] M. Bertero, T. Poggio, and V. Torre, "Visual shape computation," *Proceeding of the IEEE*, vol. 76, pp. 869–899, Aug. 1988.
- [13] C. H. Reinsch, "Smoothing by spline functions," *Numerische Mathematic*, vol. 10, pp. 177–183, 1967.
- [14] R. L. Eubank, *Spline Smoothing and Nonparametric Regression*. N. Y.: Marcel Dekker, 1988.
- [15] J. Fessler and A. Macovski, "Non-parametric fixed-interval smoothing with cubic splines," 1989. Submitted to IEEE Trans. on Acoustics, Speech, and Signal Proc.